A power modulating leg mechanism for monopedal hopping

Duncan W. Haldane, Mark Plecnik, Justin K. Yim, Ronald S. Fearing

***Abstract*— New work in robotics targets the development of controllable agile motions such as leaping. In this work, we examine animal and robotic systems on the metric of *jumping agility* and find that animals can outperform the most agile robots by a factor of two. These specially adapted animals use a jumping strategy we term *power modulation* to generate more peak power for jumping than otherwise possible. A novel eight-bar revolute mechanism designed with a new linkage synthesis approach encodes the properties for power modulation as well as constraints which assure rotation-free jumping motion. We fabricate an 85 gram prototype and demonstrate that it can perform a range of jumps while constrained by a linear slide. The prototype can deliver 3.63 times more peak jumping power than the maximum its motor can produce. A simulation matched to the physical parameters of the prototype predicts that the robot can attain an agility exceeding that of the most agile animals if the actuator power is increased to 15W.**

I. Introduction

A. Jumping agility metric

To address the shortcomings of robots as agile locomotors as compared to animals, we first establish a metric upon which the agility of animal and robotic systems can be compared.

We define *jumping agility* as the product of jump frequency and jump height. Agility has units of m/s, and corresponds to the maximum achievable average vertical velocity of the jumping system while performing repeated jumps. This is an extension of recent work which defined agility as the capacity of a robot to increase its extrinsic energy in one jump, normalized by the platform mass [19]. The jump height is simply the measure of agility further normalized by the gravitational constant. By considering the frequency as well we can more clearly differentiate between jumping systems. The jump frequency is calculated as:

$$f = \frac{1}{t_f + t_s} \tag{1}$$

where f is the jump frequency, t_f is the flight time of the jumper from when it lifts off from the ground to the apogee of its leap, and t_s is the stance time of the system during which it applies power to increase its extrinsic energy. This value is calculated for a single jumping maneuver.

By defining the operation space in this way, we can compare the agility of jumping systems with a diverse range of mechanisms including wind-up jumping robots, muscle-powered accelerations in animals, and robots capable of continuous locomotion.

This material is based upon work supported by the National Science Foundation under IGERT Grant No. DGE-0903711, the NSF GRFP, NSF CMMI 1549667, and the United States Army Research Laboratory under the Micro Autonomous Science and Technology Collaborative Technology Alliance.

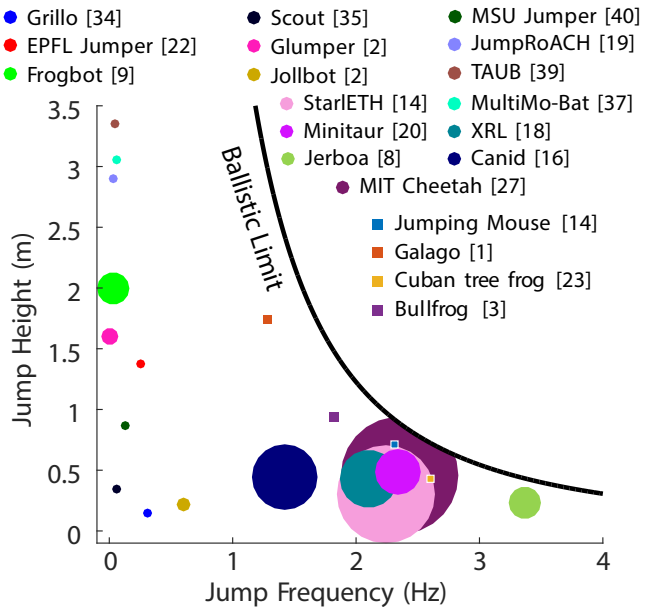

Fig. 1. Comparison chart for self-contained jumping systems. The area of the mark on the chart is proportional to mass, with a lower bound of 0.2 kg to ensure visiblity. The vertical axis is the maximum observed jump height for each platform; the horizontal axis is the jump frequency (Eqn. 1). Animal species are *G. senelgalensis* (galago), *Z. trinotatus* (Pacific jumping mouse), *O. septentrionalis* (Cuban tree frog) and *R. Catesbeiana* (Bullfrog). Neglected from this chart are all tethered robots (such as HyQ [6], and the Raibert Hopper [28]), which includes our proof of concept prototype.

Because agility is defined as a vertical climb rate in a gravitational environment, it is fundamentally limited by the power to weight ratio of the device (and has the same units). Gravity also imposes a ballistic limit on jumping systems wherein zero time is spent in stance. Fig. 1 shows a plot of jump height and jump frequency, and the ballistic limit of jumping locomotion.

For clarity we have presented the available data of each system in Fig. 1 as a single point, a jump at maximum attainable height. For wind-up robots with a mechanical escapement, this operational point is a physical constraint; however animals and robots of other actuation morphologies are not so limited. A controllably agile system will be able to operate in a region on this chart, performing a wide range of agile maneuvers (as shown in Fig. 9).

B. Actuation strategies for jumping

The data from Fig. 1 are also presented in Table I, sectioned by the mechanical strategy used to transfer energy

TABLE I
JUMPING ENERGY DELIVERY MECHANISMS

Mechanism	**Robots** (*agility* (m/s))	**Animals** (*agility* (m/s))
Stiff connection	**1.12** [19], 1.07 [26] , 0.36 [6]	–
Catch mechanism	**0.34** [21], 0.065 [9] 0.045 [33] 0.13, 0.0037 [2], 0.12 [38] 0.042 [23], 0.019 [34] 0.10 [18] 0.16 [37] 0.19 [36]	**0.64** [35]
Series Elastic	**0.89** [17], 0.67 [13] 0.64 [15], 0.77 [8]	0.89 [7], **1.1** [16]
Power modulation	*This work* **2.8** (Predicted)	**2.2** [1] , 1.1 [22] 1.6 [14], 1.7 [3]

from actuators to the center of mass. The agility for each system is presented as well. The data in this table do not constitute a complete review of all systems, but are extensive enough to allow comparison, as discussed next.

Several legged platforms have what can be considered a rigid connection of the actuator to the output of the leg, using hydraulics as in HyQ [6], the Raibert hopper [28], or torque-dense DC motors in the MIT robot Cheetah [26], and Minitaur [19]. With this strategy, power flows directly from the actuator to the appendage with negligible modulation by system compliance. The Minitaur has the highest jumping agility of this class at 1.12 m/s.[1] This is the highest agility of any robotic system in Fig. 1. There are no animal systems with an analogous strategy; all muscle-tendon complexes have significant compliance (which improves jumping performance).

Catch mechanisms are most commonly used by small jumping systems, such as insects or wind-up robotic platforms. In a catch mechanism, a relatively small actuator with a large mechanical reduction slowly energizes an elastic structure which is connected in parallel with the jumping appendage. Once the structure is loaded, the energy is released by an either passive (e.g. cam escapement [21]) or active (SMA clutch [36]) trigger. This explosive release of energy means that catch mechanisms deliver power at much higher levels than the actuator can produce. We term the ratio of the peak power delivered to the foot to the maximal sustainable motor power the *power modulation factor*[2]. The disadvantage of this method of actuation is that it is hard to achieve fine-grained force control due to the potentially discontinuous input provided by the trigger, in conjunction with the large amount of parallel elasticity. Robots with catch mechanisms populate the region of Fig. 1 near the vertical axis. No system attains a jump rate greater than 1 Hz, and the highest jumping agility platform is the EPFL jumper [21] with a score of 0.34 m/s. Robots using this actuation strategy are outperformed by their animal counterparts; fleas can achieve an agility of 0.64 m/s [35].

[1]The MIT robot cheetah has nearly the same agility at 1.07 m/s, as tabulated from a video of a steeple-chase behavior by Kenneally, De and Koditschek [20]. This was implied to be an underestimate of maximal performance.

[2]This is referred to as power amplification in the biological literature, a misnomer.

Series elastic actuators have an elastic element attached in series with a rigid actuator. This elastic element stores and returns energy, allowing the actuator to develop power which can instantaneously exceed the maximum power limit of the motor. This power modulation factor is limited to 1.436 for any series elastic actuator with a linear spring [12] (numerically estimated as 1.4 by Paluska and Herr [25]), or approximately 2.0 when including the effects of gravity [12]. This is in the absence of any mechanism which would alter the effective mechanical advantage (MA) of the actuator connected to the appendage. Many robots capable of jumping use series-elastic actuators because of these benefits:

- Stable force control
- Energy efficiency
- Isolation of motor from shock loads
- Smaller limb impedance
- Power modulation factors greater than unity

The XRHex hexapedal robot has the highest agility of the series-elastic robots for which we found data [17]. The power modulation factor for XRHex was not reported, but was approximately 1.5 for a single leg of the StarlETH robot [13], for a controller optimized for jump height [11]. We place animals which are not specialized for saltatorial locomotion[3] in this category because of the non-negligible compliance of muscle-tendon complexes. Humans have a calculated agility of 0.89 m/s [7]; guinea fowl come in somewhat higher at 1.1 m/s, and have a power modulation ratio estimated to be 2.1[4] [16].

The final category of jumping energy delivery mechanisms is that of power modulation. This strategy is used by animals specialized for saltatorial locomotion, and has not been explicitly experimentally explored in robotics. This is unfortunate, considering that some of these animals attain an agility equal to or greater than every other extant animal or robotic system. The key to animal power modulation is a variable MA mechanism which connects extensor series-elastic muscles to the jumping appendage [30][4][5]. Any robot that uses a series elastic actuator to drive a limb with a non-linear MA (such as the proposed Skipper [10]) should be capable of a power modulating behavior. Here we define MA as:

$$\text{MA} = \frac{F_{ext}}{F_A} \tag{2}$$

where F_{ext} is the external ground reaction force at the foot, and F_A is the force (or torque) developed at the actuator. A large MA means that a small actuator force creates a large force on the body, and a correspondingly large acceleration. A small mechanical advantage means that a large force at the actuator produces a small force and acceleration on the body. Power modulating systems start the beginning of their jump in a limb configuration with very low MA. This allows

[3]A locomotory mode characterized by jumping or hopping. Also termed ricochetal locomotion.

[4]Here nonlinear leg kinematics can begin to act as a power modulating mechanism, increasing the ratio.

the actuator (muscle) to transfer energy into the series elastic element (tendon) without considerable motion of the body. This extends the duration of stance, allowing the motor to apply power over a longer duration. As the leg extends, the MA increases, allowing energy stored in the spring to be transferred to the extrinsic energy of the center of mass, as spring force decreases with relaxation.

This strategy allows much larger power modulation ratios than are achievable using a non-specialized series elastic actuator; Cuban tree frogs [22] have a power modulation ratio of 7, and *G. senegalensis*, the lesser bush-baby, with the highest observed jumping agility of 2.24 m/s has a power modulation ratio of 15 [1]. The power modulation strategy allows highly agile motions in animals while maintaining all the benefits of a series elastic actuator. This motivates investigation of this strategy for creating agile robotic motion. Monopedal robots have been used in the past to prove concepts related to locomotion, starting with Raibert's hopper [29] (for a review, see Sayyad et al. [32]). Motivated by this work, we seek to demonstrate the power modulating concept using a monopedal hopping robot.

C. Overview

Section II describes the design methodology used to create a jumping robotic leg utilizing a power modulating strategy. Simulation tools are used to predict robot behavior and tune design parameters in Section II-A, and II-B describes a linkage synthesis procedure which encodes all the design specifications into a single planar revolute mechanism which is then further optimized. We also establish design constraints for any jumping leg, which prevent body rotation during take off. We then explore how the MA in the energy storage phase and spring stiffness of a power modulating leg affect the jumping performance in Section II-C. The creation of a physical prototype for testing the concept is described in Section II-D, with the experimental setup. Results of the robotic experiments and simulation studies are presented in Section III.

II. Methods

In this section we describe design methods used to create a robotic leg which uses the power modulation strategy. Our goal was to create a lightweight and robust device which satisfies all design specifications. The final appendage is a singly actuated one degree of freedom eight-bar linkage which uses only revolute joints. The physical prototype of the mechanism can be seen in Figs. 4(c) and 6.

A. Simulation

We use a dynamic simulation to evaluate the properties of our designed linkages. We determine Newton's equations of motion by describing linkages as trees of bodies connected by pin joints. Root bodies retain their full six translational and rotational states while child body states are simplified to joint coordinates. Loop-closure constraints are applied to handle closed kinematic chains. Ground contact is modeled as an asymmetric spring-damper with a spring constant

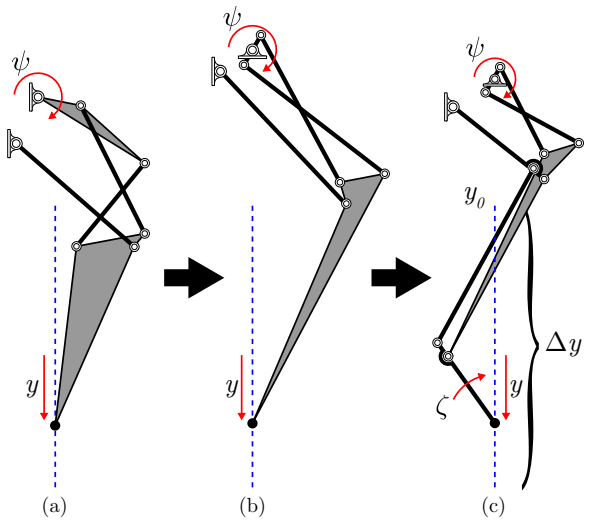

Fig. 2. (a) An initial exploration of linkage designs focused on generating a straight line along distance y. (b) Six-bar optimization allowed specification of MA by coordinating y and ψ. (c) Eight-bar optimization added momentum balancing by coordinating y, ψ, and ζ.

of 10^4 N/m and damping coefficient 50 Ns/m. Horizontal friction is modelled as approximate stick-slip friction with a coefficient of static friction of 0.5.

Our actuator model is a linear DC motor (with inertia and back EMF), driven by a voltage and current limited input. The actuator model is characterized by the motor free-running speed, torque constant, and stall current at the peak supply voltage as well as the thermally limited maximum input current.

Friction is modeled as a resistive torque applied between the crank and the body. We matched friction parameters in the simulation to experimental measurements taken after construction of the device. Observations of dry friction torque were described by the relation:

$$\tau_F = C_1 \tau_{sp} + C_2$$

where τ_{sp} is the applied torque, $C_1 = 0.045$ and $C_2 = 0.015$Nm.

B. Linkage Synthesis

To design a power modulating mechanism, we investigated the space of planar linkages with only revolute joints. Sliders, cams, and gears were avoided to save weight and complexity. We seek to determine the simplest linkage topology which can satisfy all constraints while leaving the design space open for optimization. All four-bar linkages which generate straight line motion have pivots (joints between links in mechanism) in inconvenient locations [24], and few free design parameters. We therefore expanded consideration to single degree-of-freedom six-bar linkages.

We used a design procedure [27] that fully explores the space of Stephenson path generating linkages, providing hundreds of candidate linkage designs that serve as an atlas of useful start points for an optimization procedure.

From this atlas, we selected the design shown in Fig. 2(a) which produces straight line motion with compact geometry

and an input crank that rotates 217°. To specify MA, a gradient descent optimization scheme was formulated to coordinate the input angle ψ to toe height y. The low MA required for power modulation is shown as the *Energy storage phase* in Fig. 3. For the rest of the stroke, we elected to specify a constant ground reaction force to avoid damage-causing impulsive acceleration profiles [2]. The average value of this portion of the stroke ensures that all stored energy is returned.

To compute the MA profile for constant force, we consider three configuration variables: the angle of the motor shaft, the angle of the input crank ψ, and the toe travel y. To simplify calculations, we consider a mean scenario where the motor holds an angle of ψ_{eq} for all time, the crank rotates from ψ_{max} to ψ_{eq}, and the toe translates from y_0 over a distance Δy. The input-output function is $\psi = g(y)$ of which its derivative with respect to y i.e. $g'(y)$ is identically MA. We require $g'(y)$ such that it multiplies by an unwinding spring torque to produce a constant output force F,

$$-k\big(g(y)-\psi_{\text{eq}}\big)g'(y) = F, \tag{3}$$

with k as stiffness. The solution to this ordinary differential equation is

$$g(y) = (\psi_{\text{max}} - \psi_{\text{eq}})\sqrt{1-\frac{y-y_0}{\Delta y}} + \psi_{\text{eq}}. \tag{4}$$

MA is shown in Fig. 3 as the target curve.

In addition to having the capacity for power modulation, we also specify that the jumping appendage generates no body rotation when jumping, or while extending the leg in the air. This decouples control of the body's angular momentum from motion of the leg and allows a smaller reorientation actuator to control rotation through a mechanism like an inertial tail. This strategy is in contrast to approaches that control both launch energy and angular momentum with one actuator, as the proposed Skipper robot does [10].

Previous work has addressed rotation minimization by optimizing the parameters of a four-bar leg such that the angular impulse generated during a single jump was minimized [23]. This approach is not extensible to a jumping appendage that performs a range of agile maneuvers. If the leg lifts off early, or at a different velocity the net angular impulse may not be zero. For our jumper, each 1% of launch energy (assuming a 1 joule jump) that bleeds into rotational kinetic energy produces 12 rad/s of angular velocity, making landings difficult. We therefore seek to define a set of conditions such that no angular impulse is generated by the jumping mechanism.

The fundamental constraint is that the ground reaction force generated by the mechanism always passes through the center of mass of the system. This behavior may be specified in a number of ways; we select the trivial case wherein the foot travels in a straight line. This line passes through the center of gravity of the body the leg is attached to, and the center of gravity of the moving jumping mechanism also falls on this line. To further decouple the action of the jumping mechanism from rotational dynamics, we stipulate

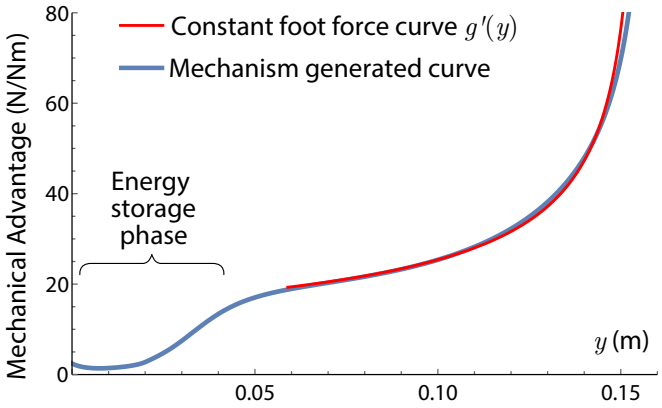

Fig. 3. The variable MA of the robot's leg mechanism starts with an energy storage phase near singularity (low mechanical advantage) at the top of stroke, then transitions to follow a constant foot force curve.

that the angular momentum of the moving links is balanced. If this constraint were not met in a zero external moment environment (i.e. while airborne), the robot body would rotate to some angle dependent on the extension of the leg.

Optimization was performed on the design variables, $\mathbf{d}$, a vector of dimension 16 containing the coordinates of pivots and the toe point in a reference configuration defining dimensions of the linkage. Formulating vector loop equalities $\mathcal{C}_j$ for each position j creates constraints between $\mathbf{d}$, the unknown toe coordinates (x_j, y_j), and input crank angles ψ_j, $j = 1, \ldots, N-1$. The objective function is the weighted sum of squared differences between the desired and actual constrained values of these unknowns,

$$\begin{aligned} f =& w_{\text{pt}} \sum_{j=0}^{N-1} \Big((\tilde{x}_j - x_j)^2 + (\tilde{y}_j - y_j)^2 \Big) + \\ & w_{\text{ang}} \sum_{j \in l} \Big((\cos\tilde{\psi}_j - \cos\psi_j)^2 + (\sin\tilde{\psi}_j - \sin\psi_j)^2 \Big) \end{aligned} \tag{5}$$

where the tilde accent indicates specified desired values. The set l contains the indices of configurations where $\tilde{\psi}_j$ was specified. Symbols w_{pt} and w_{ang} are weights. Equality and inequality constraints were placed on the elements of $\mathbf{d}$ to enforce packaging requirements, which are denoted as set $\mathcal{D}$. The optimization problem is then

$$\begin{aligned} \min \quad & f(x_j, y_j, \psi_i), \;\; j = 0, \ldots, N-1, \; i \in l \\ \text{subject to} \quad & \mathcal{D}, \; \mathcal{C}_j, \;\; j = 1, \ldots, N-1 \end{aligned} \tag{6}$$

The optimization procedure resulted in the design shown in Fig. 2(b) which was prototyped using a fixed spring to drive leg extension, shown in Fig. 4(a). Test jumps of the prototype resulted in an angular velocity of 24.8 rad/s upon leaving the ground, (Fig. 4(b)). This was due to inaccuracies in our initial estimates for link masses, the real link masses violated the assumption that all leg mass would be balanced on the line of action.

The arrangement of links in design 2(b) made achieving this balance difficult. The ternary link had mass concentrated away from the body, and all links possess negative angular

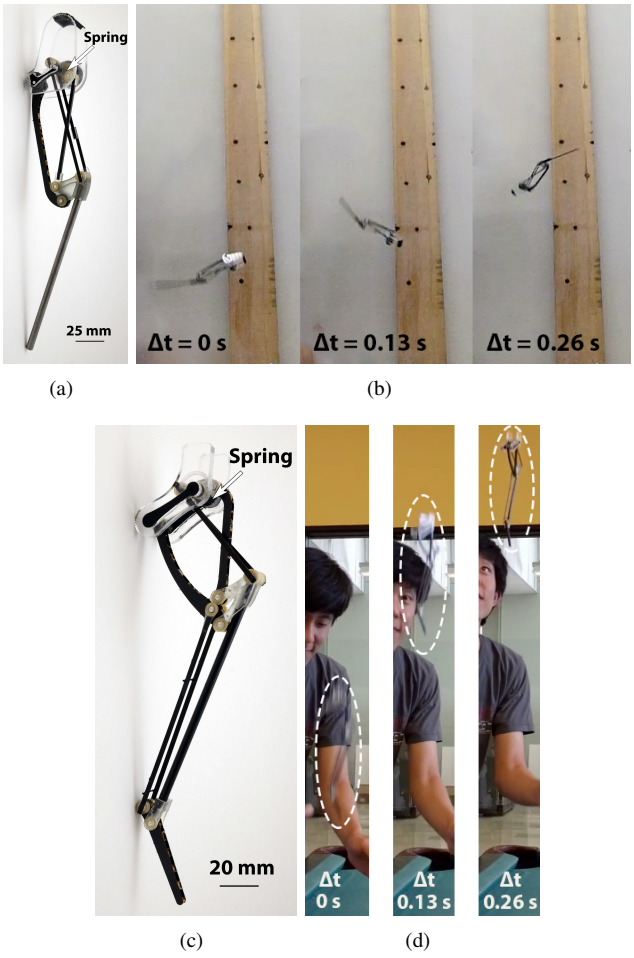

Fig. 4. (a) Image of the spring driven 6-bar (b) Stills from a high-speed video showing a rapid body rotation of 24.8 rad/s. (c) Image of the 8-bar leg mechanism (d) a spring powered jump with zero rotation.

momentum about the center of mass. These problems were countered by adding a new foot link to the mechanism which was constrained by a second floating link, making the overall mechanism a single degree-of-freedom eight-bar. The addition of these links coarsely balanced momentum but disrupted the straight line, power modulation, and constant force requirements. In order to re-satisfy these requirements, an eight-bar optimization scheme was similarly formulated that allowed coordination of y, ψ, and rotation of the foot ζ to implement momentum balancing, which produced the final kinematic design which is shown in Fig. 2(c). We fabricated a spring-driven prototype of this design (Fig. 4(c)) to validate that the balancing procedure was successful. Jump experiments confirmed that there was no rotation produced by the action of the jumping mechanism, as shown in Fig. 4(d). The obtained MA of this linkage is shown in Fig. 3 as the mechanism generated curve.

C. Mechanical Power Modulation

A power modulating mechanism is a series elastic actuator attached to a limb with variable MA. The low MA in the energy storage phase enhances its capacity for energy storage; high average MA during leg extension ensures

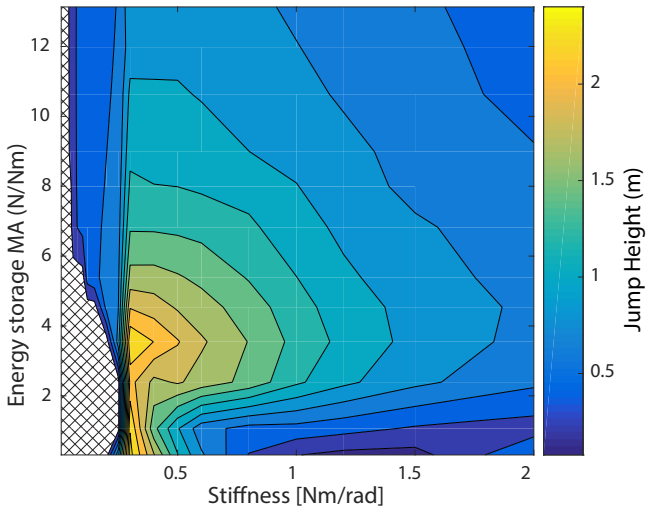

Fig. 5. Parameter sweep for energy storage phase MA and spring stiffness evaluated for jump height for an 85 gram, 25W jumping robot. The robot is unable to jump in the hatched region.

rapid and complete energy return. The degree of energy storage (and the power modulation factor) has a multivariate dependence on the parameters of the series elastic actuator and the MA function.

Fig. 5 evaluates jump height for two of these parameters: (1) spring stiffness and (2) mechanical advantage in the energy storage phase. The latter refers to MA at the beginning of the stroke which was modified by adjusting the initial configuration of the mechanism according to Fig. 3. Jump height data were determined by simulating mechanisms from a range of energy storage phase MAs and spring stiffnesses. In these simulations of maximum jump height, the mechanism is constrained to move only vertically, the energy return phase MA function is held fixed (with an average value of 26.9 N/Nm), the current input is held at maximum, the motor is a DC actuator model producing a maximum of 25W of power, and the platform weight is 85 grams.

The highest jumps in Fig. 5 are found with 0.3 Nm/rad spring stiffness and energy storage phase mechanical advantage $\approx$ 4 N/Nm. With these parameters, the robot remains in the energy storage phase (the region of low mechanical advantage marked in Fig. 3 from $0 < y <\approx 0.05$) long enough to transfer significant energy into the spring element. With stiffness less than the optimal value of 0.3 Nm/rad, the robot fails to lift off the ground. For this case, due to a low series spring stiffness, the motor is operating at high velocity and low torque, and the motor torque acting through the mechanical advantage applies a foot force less than or equal to the robot weight. Alternatively, with M.A. of 4 N/Nm and stiffness greater than 0.3 Nm/rad, the jumping performance decreases, as with less energy stored in the spring, the jump height is more dominated by the power of the actuator instead of any power modulating effects. In the limiting case of no series elastic element, the peak power applied is solely the motor peak power.

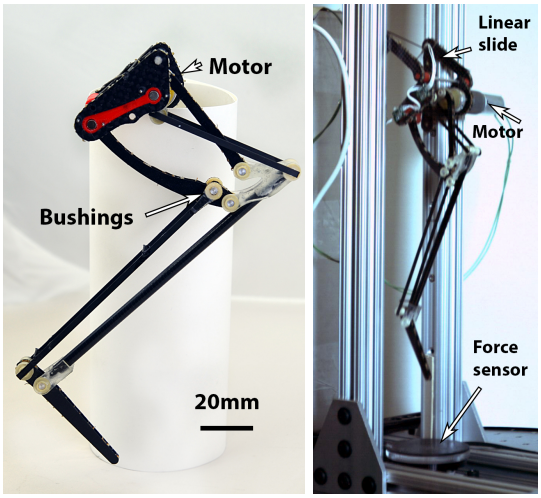

(a) (b)

Fig. 6. (a) The power modulating leg mechanism, and (b) jumping on the test stand in a still taken from a high-speed video.

D. Robotic prototype and experimental setup

The motor driven version of the power modulating leg is shown in Fig. 6(a). Aiming to minimize the moving mass of the linkage, we made as much of the mechanism as possible out of pre-fabricated carbon-fiber materials. We first simulated the mechanism jumping to its maximum attainable height of 2.2m, and recorded the resulting internal forces. The binary and ternary links subject to compressive loads are milled from carbon-fiber sandwich panel with a Nomex honeycomb core using a grout-routing Dremel bit installed in an Othermill. The two binary links subject to tension are comprised of slender uni-directional carbon fiber tie rods. The quaternary link is comprised largely of a single carbon fiber tube.

The revolute joints of this robot are made using polymer bushings (*IGUS JFM-0304-05*) reamed and trimmed to accept 0.125" diameter precision ground 2024 Aluminum shaft. This choice saves weight over the alternative ball bearings, and precludes platform failure resulting from brinelling in the impact loaded joints. To connect the bushings to the structural carbon fiber, we use small pieces of molded polyurethane (*IE-3075, Innovative Polymers*). The input crank is entirely made from this material. As a result of this design methodology, the moving mass of the entire mechanism totals only 10.8 grams despite withstanding internal loads up to 200N.

The elastic energy storage element in the power modulating leg is a torsional spring attached between the motor output and crank. We adopt the conic-sectioned latex element developed for the CMU series elastic snake [31] as our spring. Latex has by far the greatest energy density of commonly available materials, as well as a high resilience. We cut our springs from latex tube stock fabricated with a continuous-dip process (*Primeline Industries*) using a 3D printed jig. The final spring has an active latex mass of 1.5 grams, and a total mass (with attachment features) of 2.5 grams. The stiffness of the spring on the prototype was estimated at 0.45 Nm/rad during experiments; somewhat stiffer than the optimum (Fig. 5).

Our target platform mass is 85 grams, of which the leg and spring claim 13.3, leaving just over 70 grams for actuation, and attachment to the experimental test stand.

We used a low-power, low-cost, off-the-shelf geared motor (*Pololu 20D 154:1*) to test the operating principle of the power modulating leg. This motor weighs 46.9 grams, including the mounting hub. It offers little in the way of control authority, but was readily accessible and demonstrates the power-modulating properties of the robotic leg. The total mass of the robot including leg, body and actuator is 73.4 grams.

Our driven jumping experiments were performed with the robot attached to a vertically-oriented linear slide rail which increased the mass of the robot to 84.8 grams, shown in Fig. 6. The leg is free to rotate in pitch on the linear slide carriage. This carriage contributed significant friction in our experiments; there was little room in the mass budget to rigidify the carriage, and any off-axis forces tended to cause jamming issues. To collect data, we logged angle information from two AS5048B magnetic encoders mounted on the ternary carbon fiber link, and motor output, the current of the motor as sensed by a shunt resistor, and the ground reaction force from an ATI Nano43 force sensor, which served as the jumping platform. The force sensor was covered in neoprene rubber to isolate it from shock loads. 1080p video footage of each experiment was recorded at 500 frames per second.

To explore the range of jump heights this robot can attain, we commanded a set of open-loop motor commands in lieu of a closed-loop controller. The robot was set in a starting position with a MA larger than the minimum attainable by the mechanism, which limits the jump height and power modulating capacity of the linkage, as shown in Fig. 5. However, this configuration $\psi = g(y)$ was necessary to overcome friction generated by the linear slideway.

III. Results

In this section we present results from robot experiments and simulation. The robot mass was set to be 85 grams in simulation to match the experimental platform. Fig. 7 compares the spring and motor power for the simulation vs an experimental jump of the robotic leg. Power is calculated by taking the product of the torque deflecting the spring and the angular velocity of the crank or motor, for spring and motor power respectively. The simulation shows good correspondence with the experiment. The power modulating mechanism allows the spring to deliver a peak power of 11.4 W, with the motor delivering an estimated maximum of 3.14W, for an instantaneous power modulation factor of 3.63. This factor is lower than the maximum attainable (see Fig. 8) in simulation because the robot was not started in its minimum MA position. Friction in the mechanism and slideway resulted in lower peak spring power observed in experiments than the simulation predicted.

We explore the effect of power input level on the power modulating mechanism using a simulation matched to the

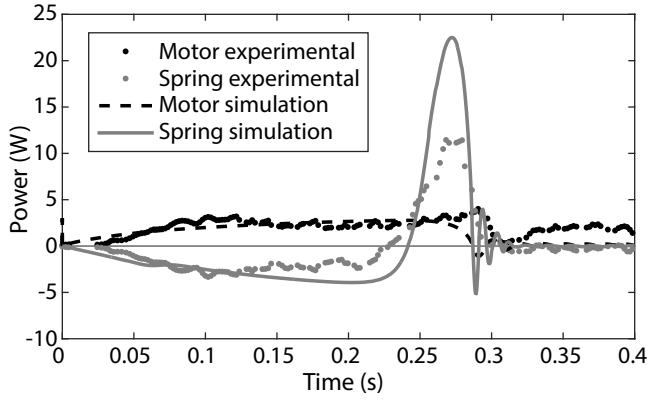

Fig. 7. Simulated vs measured power for the 3W actuator installed in the prototype.

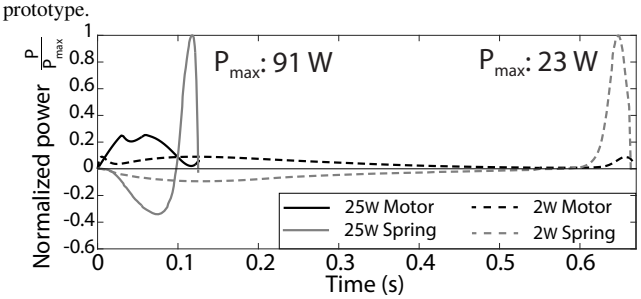

Fig. 8. Normalized motor and spring power for simulated actuators producing a maximum power of 25W and 2W.

physical parameters of the robot. For each of these simulations, we fix the maximum torque input and vary the maximum speed of a virtual actuator.

Fig. 8 shows the normalized power from the motor and spring during a simulated jump of the leg, as a function of stance time for power input levels of 25W and 2W. The power modulating properties of the linkage are clear for both power input levels. A 25W input to the leg yields a power modulation ratio of 3.6; a 2W input has a much higher ratio of 11.5. The time for the jumping leg to lift off decreases with increasing actuator power, indicating that jumps can be made more frequently with a higher-power actuator.

Fig. 9 shows the achievable operational space of the jumping linkage for a range of power inputs to the power modulating leg. These axes are identical to those of the comparison chart shown in Fig. 1. Zones of operation were determined by exploring the range of attainable jumps in simulation using open-loop motor commands. This exploration yielded a pareto-optimal set in the operational space. The operating region is defined as the projection of the set of pareto-optimal jumps to the horizontal axis; physically this means that any jump that can be made quickly can also be made slowly by delaying the onset of actuation. The simulation predicts that the robot can make controlled, repeatable jumps anywhere in these zones of operation.

The greater the level of power input to the leg, the more agile the system becomes and the greater the attainable jump height, up to a maximum of 2.2m at a power input level of 15W. We found that no significant gains in jump height are expected by further increasing the power to 25W;

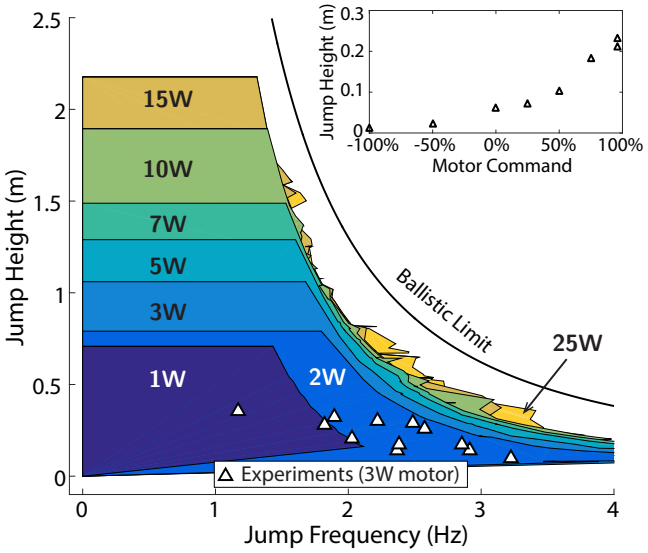

Fig. 9. The achievable operational space of the power modulating mechanism for a range of power inputs. Also shown are experimentally observed jumps with the leg prototype. *Inset:* Experimental data showing jump height as a function of motor command, the motor input specified as a fraction of maximum voltage applied during the second phase of the jump. Both figures created for the 85 gram jumping platform.

the increased operational space only appears as a slight expansion of higher frequency motion.

Also shown in this figure are experimental data gathered from the robot jumping on the test stand. Each of these data points represents the robot jumping with motor commands defined as follows: first the motor PWM command is set to 90% of full range to lift the mechanism out of the low MA region. When the mechanism is almost out of this region, the motor command changes to a fixed constant value from -100% to +100% PWM duty cycle. Varying the motor command causes the robot to jump to various heights, as shown in the inset of Fig. 9. Increasing motor commands lead to a corresponding increase in jump height. The experimental data falls within the envelope expected for a 3W power level. The jump height observed in experiments falls below the predicted maximum, which is a combined effect of a spring that was stiffer than predicted (see Fig. 5), exacerbated by friction and jamming in the linear slideway. The maximum agility was 0.71 m/s; this value is not shown in Fig. 1 because the robot drew power from a tether.

IV. Conclusion and Future Work

In this work we investigated the operational space of agile motion for animals and robotic systems. Comparing the systems on the metric of *jumping agility* showed that some animals adapted for saltatorial locomotion can outperform any extant robotic system by a factor of two. The limbs of some of these animals have a MA profile which allows the production of greater peak jumping power than would otherwise be possible. This strategy, termed power modulation, had not yet been explicitly employed by a robotic system so we developed a monopedal hopping robot to demonstrate the principle. A new linkage synthesis approach was used to encode the power modulating properties into a

planar revolute eight-bar jumping mechanism. The linkage was fabricated and coupled with a torsional spring element and brushed DC motor to create a monopedal hopper, from which was collected experimental data.

These data showed that the power modulating leg could instantaneously deliver 3.63 times more power than the steady-state maximum of the motor. In addition to demonstrating the principle of power modulation for agile robots, we show that the robot is capable of performing a range of jumps to different heights by varying only motor commands. This demonstrates more controllability for power modulating mechanisms than has been demonstrated for robots with catch mechanisms. We use a simulation matched to the physical parameters of the robotic platform to explore how the performance of the power modulating leg varies as more actuator power is made available. If we increase the power available to the actuator to 15W, then the simulation predicts that the robot should attain an agility of 2.85 m/s, on par with the most agile animal for which we have data. This prediction assumes that frictional properties in the mechanism are scale invariant with respect to power input. These results may not be immediately achievable, but the degree of predicted improvement indicates that further study is merited.

The next phase of this research is to incorporate a higher power density actuator to validate experimentally that we can attain the agility predicted by the simulation, and to remove the confounding factors created by the linear slide way.

REFERENCES

[1] P. Aerts, "Vertical jumping in Galago senegalensis: the quest for an obligate mechanical power amplifier," *Philos. Trans. R. Soc. B Biol. Sci.*, vol. 353, no. 1375, pp. 1607–1620, 1998.

[2] R. Armour, K. Paskins, A. Bowyer, J. Vincent, W. Megill, and R. Bomphrey, "Jumping robots: a biomimetic solution to locomotion across rough terrain," *Bioinspir. Biomim.*, vol. 2, no. 3, pp. S65–82, 2007.

[3] H. C. Astley, E. M. Abbott, E. Azizi, R. L. Marsh, and T. J. Roberts, "Chasing maximal performance: a cautionary tale from the celebrated jumping frogs of Calaveras County," *J. Exp. Biol.*, vol. 216, no. Pt 21, pp. 3947–3953, 2013.

[4] H. C. Astley and T. J. Roberts, "Evidence for a vertebrate catapult: elastic energy storage in the plantaris tendon during frog jumping," *Biol. Lett.*, vol. 8, no. 3, pp. 386–389, 2012.

[5] ——, "The mechanics of elastic loading and recoil in anuran jumping," *J. Exp. Biol.*, vol. 217, no. 24, pp. 4372–4378, 2014.

[6] T. Boaventura, C. Semini, J. Buchli, M. Frigerio, M. Focchi, and D. G. Caldwell, "Dynamic torque control of a hydraulic quadruped robot," *IEEE Int. Conf. Robot. Autom.*, pp. 1889–1894, 2012.

[7] M. F. Bobbert, "Dependence of human squat jump performance on the series elastic compliance of the triceps surae: a simulation study," *J. Exp. Biol.*, vol. 204, no. 3, pp. 533–542, 2001.

[8] A. Brill, A. De, A. Johnson, and D. Koditschek, "Tail-assisted rigid and compliant legged leaping," *IEEE Int. Conf. Intell. Robot. Syst.*, pp. 6304–6311, 2015.

[9] J. Burdick and P. Fiorini, "Minimalist jumping robots for celestial exploration," *Int. J. Rob. Res.*, vol. 22, no. 7-8, pp. 653–674, 2003.

[10] J. Driessen, "Machine and behaviour co- design of a powerful minimally actuated hopping robot," Masters, TU Delft, 2015.

[11] P. Fankhauser, M. Hutter, C. Gehring, M. Bloesch, M. A. Hoepflinger, and R. Siegwart, "Reinforcement learning of single legged locomotion," *IEEE Int. Conf. Intell. Robot. Syst.*, pp. 188–193, 2013.

[12] A. Galantis and R. C. Woledge, "The theoretical limits to the power output of a muscle-tendon complex with inertial and gravitational loads," *Proc. R. Soc. B Biol. Sci.*, vol. 270, no. 1523, pp. 1493–1498, 2003.

[13] C. Gehring, S. Coros, M. Hutter, and R. Siegwart, "An optimization approach to controlling jump maneuvers for a quadrupedal robot," *Dyn. Walk. Conf.*, 2015.

[14] T. H. Harty, "The Role of the Vertebral Column during Jumping in Quadrupedal Mammals." Ph.D. dissertation, Oregon State University, 2010.

[15] G. C. Haynes, J. Pusey, R. Knopf, A. M. Johnson, and D. E. Koditschek, "Laboratory on legs: an architecture for adjustable morphology with legged robots," University of Pennsylvania, Philidelphia, PA, Tech. Rep., 2012.

[16] H. T. Henry, "Performance of guinea fowl Numida meleagris during jumping requires storage and release of elastic energy," *J. Exp. Biol.*, vol. 208, no. 17, pp. 3293–3302, 2005.

[17] A. M. Johnson and D. E. Koditschek, "Toward a vocabulary of legged leaping," *IEEE Int. Conf. Robot. Autom.*, pp. 2568–2575, 2013.

[18] G.-P. Jung, C. S. Casarez, S.-P. Jung, R. S. Fearing, and K.-J. Cho, "An integrated jumping-crawling robot using height-adjustable jumping module," *IEEE Int. Conf. Robot. Autom.*, pp. 4680–4685, 2016.

[19] G. Kenneally, A. De, and D. E. Koditschek, "Design principles for a family of direct-drive legged robots," *IEEE Robot. Autom. Lett.*, vol. 1, no. 2, pp. 900–907, 2016.

[20] ——, "Design principles for a family of direct-drive legged robots," *Robot. Sci. Syst. Work.*, pp. 17–19, 2015.

[21] M. Kovač, M. Schlegel, J.-C. Zufferey, and D. Floreano, "Steerable miniature jumping robot," *Auton. Robots*, vol. 28, no. 3, pp. 295–306, 2009.

[22] R. L. Marsh and H. B. John-Alder, "Jumping performance of hylid frogs measured with high-speed cine film," *J. Exp. Biol. Biol.*, vol. 188, pp. 131–41, 1994.

[23] M. Noh, S.-W. Kim, S. An, J.-S. Koh, and K.-J. Cho, "Flea-Inspired Catapult Mechanism for Miniature Jumping Robots," *IEEE Trans. Robot.*, vol. 28, no. 5, pp. 1007–1018, 2012.

[24] H. Nolle, "Linkage coupler curve synthesis: A historical review - I. Developments up to 1875," *Mech. Mach. Theory*, vol. 9, no. 2, pp. 147–168, 1974.

[25] D. Paluska and H. Herr, "The effect of series elasticity on actuator power and work output: Implications for robotic and prosthetic joint design," *Rob. Auton. Syst.*, vol. 54, no. 8, pp. 667–673, 2006.

[26] H.-w. Park, P. M. Wensing, and S. Kim, "Online planning for autonomous running jumps over obstacles in high-speed quadrupeds," *Robot. Sci. Syst.*, 2015.

[27] M. M. Plecnik and J. M. McCarthy, "Design of Stephenson linkages that guide a point along a specified trajectory," *Mech. Mach. Theory*, vol. 96, pp. 38–51, 2016.

[28] M. H. Raibert, H. B. Brown, and M. Chepponis, "Experiments in balance with a 3D one-legged hopping machine," *Int. J. Rob. Res.*, vol. 3, no. 2, pp. 75–92, 1984.

[29] M. H. Raibert and H. B. Brown, "Experiments in balance with a 2D one-legged hopping machine," *ASME J. Dyn. Syst. Meas. Control*, vol. 106, pp. 75–81, 1984.

[30] T. J. Roberts and R. L. Marsh, "Probing the limits to muscle-powered accelerations: lessons from jumping bullfrogs," *J. Exp. Biol.*, vol. 206, no. 15, pp. 2567–2580, 2003.

[31] D. Rollinson, S. Ford, B. Brown, and H. Choset, "Design and Modeling of a Series Elastic Element for Snake Robots," in *ASME DSCC*, 2013.

[32] A. Sayyad, B. Seth, and P. Seshu, "Single-legged hopping robotics research - A review," *Robotica*, vol. 25, no. 05, pp. 587–613, 2007.

[33] U. Scarfogliero, C. Stefanini, and P. Dario, "Design and Development of the Long-Jumping " Grillo " Mini Robot," no. April, pp. 10–14, 2007.

[34] S. A. Stoeter, P. E. Rybski, M. Gini, and N. Papanikolopoulos, "Autonomous stair-hopping with scout robots," *IEEE Int. Conf. Intell. Robot. Syst.*, vol. 1, pp. 721–726, 2002.

[35] G. P. Sutton and M. Burrows, "Biomechanics of jumping in the flea." *J. Exp. Biol.*, vol. 214, no. Pt 5, pp. 836–47, 2011.

[36] M. A. Woodward and M. Sitti, "MultiMo-Bat: A biologically inspired integrated jumping-gliding robot," *Int. J. Rob. Res.*, vol. 33, pp. 1511–1529, 2014.

[37] V. Zaitsev, O. Gvirsman, U. Ben Hanan, A. Weiss, A. Ayali, and G. Kosa, "Locust-inspired miniature jumping robot," *IEEE Int. Conf. Intell. Robot. Syst.*, vol. 2015-Decem, no. 6, pp. 553–558, 2015.

[38] J. Zhao, N. Xi, B. Gao, M. W. Mutka, and L. Xiao, "Development of a controllable and continuous jumping robot," *IEEE Int. Conf. Robot. Autom.*, pp. 4614–4619, 2011.